Periodic nonlinear Fourier transform for fiber-optic communications, Part II: Eigenvalue communication

MORTEZA KAMALIAN,[*] JAROSLAW E. PRILEPSKY,[†] SON THAI LE, AND SERGEI K. TURITSYN[‡]

Aston Institute of Photonic Technologies, Aston University, B4 7ET Birmingham, UK
[†]*y.prylepskiy1@aston.ac.uk*
[‡]*s.k.turitsyn@aston.ac.uk*
[*]*kamaliam@aston.ac.uk*

Abstract: In this paper we propose the design of communication systems based on using periodic nonlinear Fourier transform (PNFT), following the introduction of the method in the Part I. We show that the famous "eigenvalue communication" idea [A. Hasegawa and T. Nyu, J. Lightwave Technol. **11**, 395 (1993)] can also be generalized for the PNFT application: In this case, the main spectrum attributed to the PNFT signal decomposition remains constant with the propagation down the optical fiber link. Therefore, the main PNFT spectrum can be encoded with data in the same way as soliton eigenvalues in the original proposal. The results are presented in terms of the bit-error rate (BER) values for different modulation techniques and different constellation sizes vs. the propagation distance, showing a good potential of the technique.

OCIS codes: (060.1660) Coherent communications; (060.2330) fiber optics communications; (070.4340) Nonlinear optical signal processing.

References and links

1. S. Wahls and H. V. Poor, "Fast numerical nonlinear Fourier transforms," IEEE Trans. Inf. Theory **61**, 6957–6974 (2015).
2. A. Hasegawa and T. Nyu, "Eigenvalue communication," J. Lightwave Technol. **11**, 395–399 (1993).
3. S. Hari, F. Kschischang, and M. Yousefi, "Multi–eigenvalue communication via the nonlinear Fourier transform," in *27th Biennial Symposium on Communications (QBSC)*, 92–95 (2014).
4. A. Maruta, Y. Matsuda, H. Terauchi, and A. Toyota, "Digital coherent technology-based eigenvalue modulated optical fiber transmission system," in *Odyssey of Light in Nonlinear Optical Fibers: Theory and Applications*, Ch. 19, edts. K. Porsezian and R. Ganapathy, pp. 491–506 (CRC, 2015).
5. A. Maruta, "Eigenvalue modulated optical transmission system (invited)," in *The 20th OptoElectronics and Communications Conference (OECC)*, Shanghai, China, Paper JThA.21 (2015).
6. Z. Dong, et al. "Nonlinear frequency division multiplexed transmissions based on NFT," IEEE Photon. Tech. Lett. **27**, 1621–1623 (2015).
7. J. E. Prilepsky, S. A. Derevyanko, K. J. Blow, I. Gabitov, and S. K. Turitsyn, "Nonlinear inverse synthesis and eigenvalue division multiplexing in optical fiber channels," Phys. Rev. Lett. **113**, 013901 (2014).
8. S. T. Le, J. E. Prilepsky, and S. K. Turitsyn, "Nonlinear inverse synthesis for high spectral efficiency transmission in optical fibers," Opt. Express **22**, 26720–26741 (2014).
9. S. T. Le, J. E. Prilepsky, and S. K. Turitsyn, "Nonlinear inverse synthesis technique for optical links with lumped amplification," Opt. Express **23**, 8317-8328 (2015).
10. E. R. Tracy and H. H. Chen, "Nonlinear self-modulation: an exactly solvable model," Phys. Rev. A **37**, 815–839 (1988).
11. G. P. Agrawal, *Nonlinear Fiber Optics,* 5th Ed. (Academic, 2013).
12. V. E. Zakharov and A. B. Shabat, "Exact theory of two-dimensional self-focusing and one-dimensional self-modulation of waves in nonlinear media," Soviet Physics-JETP **34**, 62–69 (1972).
13. S. T. Le, J. E. Prilepsky, M. Kamalian, P. Rosa, M. Tan, J. D. Ania-Castanon, P. Harper, and S. K. Turitsyn, "Optimized nonlinear inverse synthesis for optical links with distributed Raman amplification," in *41st European Conference on Optical Communications (ECOC)*, Valencia, Spain, paper Tu 1.1.3 (2015).
14. S. T. Le, J. E. Prilepsky, P. Rosa, J. D. Ania-Castanon, and S. K. Turitsyn, "Nonlinear inverse synthesis for optical links with distributed Raman amplification,"J. Lightwave Technol. **34**, 1778–1785 (2016).
15. M. Tan, P. Rosa, I. D. Phillips, and P. Harper, "Long–haul transmission performance evaluation of ultra–long Raman fiber laser based amplification influenced by second order co–pumping," *Asia Communications and*

Photonics Conference, Shanghai, China, ATh1E-4 (2014).
16. S. Wahls, S. T. Le, J. E. Prilepsky, H. V. Poor, and S. K. Turitsyn, "Digital backpropagation in the nonlinear Fourier domain," in *Proceedings of IEEE 16th International Workshop in Signal Processing Advances in Wireless Communications (SPAWC)*, Stockholm, Sweden, pp. 445-449 (2015).
17. E. R. Tracy, "Topics in nonlinear wave theory with applications," PhD Thesis, Univ. of Maryland, College Park, MD, USA (1984).
18. O. R. Its and V. P. Kotlyarov. "Explicit formulas for the solutions of a nonlinear Schrödinger equation." Doklady Akad. Nauk Ukrainian SSR, ser. A vol. 10, 965–968 (1976); English translation available at http://arxiv.org/abs/1401.4445v1.
19. A. Osborne, *Nonlinear ocean waves and the inverse scattering transform*, 1st ed. (Academic, 2010).
20. A. Bobenko and C. Klein, eds. *Computational approach to Riemann surfaces,* No. 2013, (Springer Science and Business Media, 2011).
21. M. Bertola and P. Giavedoni, "A degeneration of two-phase solutions of the focusing nonlinear Schrödinger equation via Riemann-Hilbert problems," J. Math. Phys. **56**, 061507 (2015).
22. M. Kamalian, J. E. Prilepsky, S. T. Le, and S. K. Turitsyn, "Optical communication based on the periodic nonlinear Fourier transform signal processing," *IEEE 6th International Conference on Photonics (ICP)*, Sarawak, Malaysia (2016).
23. H. Steudel and R. Meinel, "Periodic solutions generated by Bäcklund transformations," Physica D **21**, 155–162 (1986).
24. P. Poggiolini, A. Carena, V. Curri, and F. Forghieri, "Evaluation of the computational effort for chromatic dispersion compensation in coherent optical PM-OFDM and PM-QAM systems," Opt. Express **17**, 1385–1403 (2009).
25. R. A. Shafik, M. S. Rahman, and A. H. M. Islam, "On the extended relationships among EVM, BER and SNR as performance metrics," IEEE International Conference on Electrical and Computer Engineering (ICECE), pp. 408–411 (2006).
26. W. Shieh, W. Chen, and R.S. Tucker, "Polarisation mode dispersion mitigation in coherent optical orthogonal frequency division multiplexed systems," Electron. Lett. **42**, 996–997 (2006).
27. T. Hirooka and M. Nakazawa, "Linear and nonlinear propagation of optical Nyquist pulses in fibers," Opt. Express **20**, 19836–19849 (2012).
28. M. Cvijetic and P. Magill, "Delivering on the 100GbE promise (Message from the Series Editor)," IEEE Comm. Magazine **45**, 2–3 (2007).
29. M. I. Yousefi and F. R. Kschischang, "Information transmission using the nonlinear Fourier transform, part II: numerical methods," IEEE Trans. Inf. Theory **60**, 4329–4345 (2014).
30. M. I. Yousefi and F. R. Kschischang, "Information transmission using the nonlinear Fourier transform, part III: spectrum modulation," IEEE Trans. Inf. Theory **60**, 4346–4369 (2014).

1. Introduction

In the Part I of this work we described the PNFT peculiarities, introduced the most important quantities (main and auxiliary spectra) resulting from the PNFT periodic signal decomposition, and explained the differences arising when dealing with the PNFT compared to its "ordinary" counterpart — the NFT attributed to burst-mode (or truncated at the time interval boundaries) signals. We also itemized the potential advantages of using the PNFT against the burst-mode NFT in the optical transmission. Although, as it was explained in Part I, the utilization of periodic signals can bring noticeable benefits in terms of the reduction of the processing complexity and the capability of control over the generated signal time-extent, much less attention has been paid to the PNFT applications due to a more complex mathematical background involved. In this regard we would like to mention a very resent paper of Wahls and Poor [1], where a quite exhaustive survey of the PNFT theory and numerical methods including the newest fast direct PNFT decomposition algorithms, was presented, perhaps aside from the computation of theta-functions (see subsection 4.2 of our Part I). In the first part, we also analyzed the available numerical tools for the direct PNFT computation, addressing the quality of the resulting main spectrum and the associated processing time consumption, and inferred that the best performance attributes to the Ablowitz-Ladik (AL) discretization algorithm. Thus, in this Part II, whenever we present any data for the PNFT spectrum, these are computed with the use of the AL routine described in Part I, see also [1]. It is worth noting that the AL algorithm can be recast into the fast form using the fast polynomial arithmetic [1].

The main goal of Part II is to present possible design schemes for communication systems

based on the PNFT processing and to show their potential. Here, we propose proof-of-concept designs of systems that function similarly to the burst-mode eigenvalue communication [2–6], but dealing with the periodically continued waveforms and utilizing the PNFT to retrieve the data encoded on the nonlinear spectrum (NS) at the receiver. In general, one can also design the PNFT-based communication system using the nonlinear inverse synthesis idea (NIS) [7–9]: within this approach one maps the encoded data onto the NS and then synthesises the respective signal in time domain (meaning the use of the inverse PNFT for the case considered) at the transmitter, submits the new synthesized signal into the fiber and extracts data from the received signal by performing the direct transformation (i.e. the direct PNFT) together with compensation of the evolution inside the nonlinear spectral domain. However, as was mentioned in our Part I, there is still currently a lack of a generic efficient approach for dealing with the inverse PNFT, and its computation brings about technical difficulties. Therefore, to simplify the task, instead of performing the inverse transformation we use signals with the analytically known NS and, hence, bypass the inverse PNFT step in the synthesis procedure. On the other hand, the efficient AL algorithm is used at the receiver to retrieve the encoded data from the main spectrum.We numerically evaluate the performance of our PNFT-based systems through direct counting of BER comparing the transmitted and received bit streams.

The paper is organized as follows. In Section 2, we briefly describe the NS (main spectrum) calculation attributed to the PNFT, to make this Part II self-consistent. In Section 3, we introduce designs of the PNFT-based communication systems using three different signals with the known NS. These system are examined via the direct simulations of the noise-perturbed NLSE channel in Section 4: This section also contains the discussion of the emerging error sources. The results are summarised in the Conclusion section.

2. Channel model and main spectrum corresponding to PNFT signal decomposition

2.1. Channel model

We use as master model the NLSE with the account of the ASE noise (assuming an ideal Raman amplification) [11]:

$$i q_z - \frac{\beta_2}{2} q_{tt} + \gamma q |q|^2 = n(t,z), \tag{1}$$

where $q(t,z)$ is the slowly varying envelop of the electromagnetic field, $\beta_2 < 0$ is the chromatic dispersion parameter, γ is the nonlinearity (Kerr) coefficient, and $n(t,z)$ is the circularly symmetric complex Gaussian noise process introduced by amplifiers. The latter is completely characterized by the autocorrelation function [11]:

$$\left\langle n(t,z), n(t',z') \right\rangle = \alpha h f_s K_T \delta(t-t', z-z'), \tag{2}$$

where α is the fiber loss coefficient, typically $\alpha \approx 0.2$ dB/km at the carrying wavelength $\lambda_0 = 1.55$ μm, h is the Planck constant, f_s is the central frequency which we set to 193.41 THz, $K_T = 1.13$ is the photon occupancy factor, and $\delta(\cdot)$ is the Dirac delta-function. We note that the model in Eq. (1) can also be used as a leading approximation for the erbium-doped fiber amplifiers (EDFA) (see e.g. [9] and references therein). In this case, in the leading approximation one can use the averaged NLSE replacing γ with the effective nonlinearity coefficient

$$\gamma_{eff} = \frac{1}{L_{span}} \int_0^{L_{span}} \gamma e^{-\alpha z} dz = \gamma \frac{1 - e^{-\alpha L_{span}}}{\alpha L_{span}}, \tag{3}$$

where L_{span} is the length of span. A similar approach can be used in the case of non-ideal Raman amplification [13, 14]. We then normalize Eq. (1) using the following standard redefinitions:

$$\frac{t}{Ts} \to t, \qquad \frac{z}{Zs} \to z, \qquad q\sqrt{\frac{\gamma Z_s}{2}} \to q, \qquad n\sqrt{\frac{\gamma Z_s}{2}} \to n, \tag{4}$$

where T_s can be chosen as a free normalization parameter, and the respective z-scale becomes $Z_s = 2T_s^2/|\beta_2|$. The normalized NLSE reads:

$$i q_z + q_{tt} + 2q|q|^2 = n(t,z). \tag{5}$$

Note that the autocorrelation function intensity in Eq. (2) has to be renormalized as well according to the last expression in Eq. (4). Further we are going to work with periodic (in time variable) signals with the period T_0, therefore, the additional condition to Eq. (5) is imposed: $q(t,z) = q(t+T_0,z)$.

2.2. Direct PNFT and main spectrum definition

Insofar as we described the PNFT details in our Part I, Section 4.1, here we reproduce just some basic elements that are directly necessary for our further analysis and communication system design. The PNFT spectrum of a periodic signal consists of two parts: main and auxiliary spectra. The NS attributed to the PNFT signal decomposition is calculated according to the the following procedure. The first step is to form the fundamental matrix of the periodic version of Zakharov-Shabat system (ZSS) [12]:

$$\begin{bmatrix} i\partial_t & q(t,z) \\ -q^*(t,z) & -i\partial_t \end{bmatrix} \begin{bmatrix} \phi_1 \\ \phi_2 \end{bmatrix} = \lambda \begin{bmatrix} \phi_1 \\ \phi_2 \end{bmatrix}, \tag{6}$$

by finding two linearly independent ZSS solutions via the eigenfunctions $\Phi = [\phi_1, \phi_2]^T$ with the conditions set at some point t_0 [10, 17]:

$$\phi(t_0,t_0;\lambda) = \begin{pmatrix} 1 \\ 0 \end{pmatrix}, \qquad \tilde{\phi}(t_0,t_0;\lambda) = \begin{pmatrix} 0 \\ 1 \end{pmatrix}. \tag{7}$$

The monodromy matrix, M, is then defined as the value of the fundamental matrix at one period from the base point, $M = [\phi(t_0+T,t_0;\lambda), \tilde{\phi}(t_0+T,t_0;\lambda)]^T$. The main spectrum, $\mathbb{M}$, is defined as the set of points in the complex plane at which the ZSS solutions are anti-periodic or periodic. This condition leads to the expressions defining the dependence of the main spectrum on the waveform parameters [10, 17]:

$$\mathbb{M} = \{\lambda | \mathrm{Tr} M(t_0;\lambda) = \pm 2\}. \tag{8}$$

The important property of the main spectrum that one can utilize for the transmission purposes is that it remains invariant along the signal evolution within the unperturbed NLSE (for more information of the main spectrum role in the definition of the NLSE solution properties see Part I and [1, 10, 18]).

3. Eigenvalue communication

Using the PNFT it is possible to map data on the NS according to some deterministic one-to-one mapping rule, then synthesize the signal corresponding to this modulated NS in time domain, and launch the signal into the fiber; at the receiver side one uses the direct PNFT and retrieves the encoded data from the NS (see Fig. 1). Such a procedure can be understood as a variant of NIS [7–9] with the use of the PNFT. However, in spite of the fact that we know the evolution

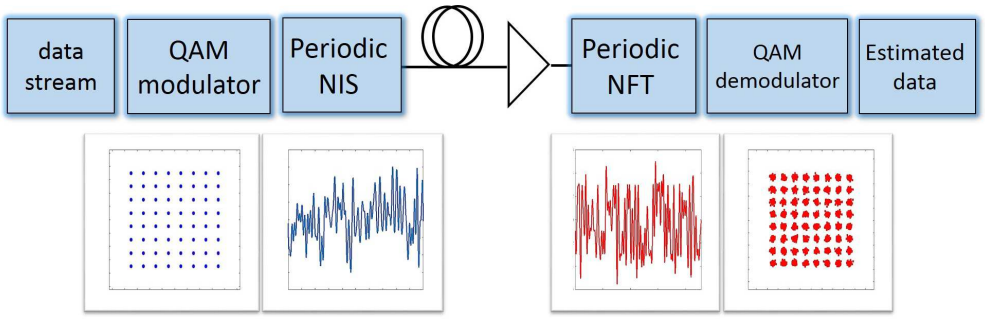

Fig. 1. General design of the NFT-based communication system concept. The data stream is mapped onto the NS (here – on the main spectrum) and then the signal is constructed from this main spectrum. At the receiver side, performing the direct transform, the original data are retrieved.

law inside the nonlinear spectral domain attributed to the PNFT, this evolution is nontrivial, in contrast to the one for the ordinary NFT, see Part I. To eliminate the evolution compensation step and simplify our system further, we can disregard the auxiliary spectrum and employ only the main spectrum part of the NS, of course, at the expense of losing some degrees of freedom available for modulation. This approach is the analogue of eigenvalue communication [2] or a variant of the nonlinear frequency division multiplexing [3]. As the main spectrum part of the NS is invariant along the signal propagation (aside from the noise-induced corruptions), one automatically circumvents the compensation of NS evolution by means of employing the main spectrum only.

3.1. *Signals with known NS*

As a simple example we select a two-phase signal with the main spectrum consisting of one complex conjugate pair of single points, λ_1 and λ_1^*, and two nearly degenerate (solution points in Eq. (8) with multiplicity of 2 as opposed to nondegenerate points with multiplicity 1) pairs, $\lambda_2, \lambda_2^*, \lambda_3$ and λ_3^*. For the case when λ_2 approaches λ_3, the periodic signal resulting from such an NS can be written as [21]:

$$q(t,z) = A\frac{\cosh(\phi z - i\sigma) + B\cos(\xi t - \alpha)}{\cosh\phi z + B\cos(\xi t - \alpha)} e^{iNz}, \tag{9}$$

where the parameters in Eq. (9) are expressed through the main spectrum eigenvalues λ_1 and λ_3 as follows

$$\begin{aligned}
&A = \mathrm{Im}\lambda_1, \quad N = -4\mathrm{Re}\lambda_1^2 - 2\mathrm{Im}\lambda_1^2, \quad \alpha = \pi,\\
&B = \frac{(|\lambda_3 - \lambda_1| - |\lambda_3 - \lambda_1^*|)^2}{|\lambda_3 - \lambda_3^*||\lambda_1 - \lambda_1^*|},\\
&\phi = -4\mathrm{Im}\left[(\lambda_3^* + \mathrm{Re}\lambda_1)\sqrt{(\lambda_3^* - \lambda_1)(\lambda_3^* - \lambda_1^*)}\right],\\
&\sigma = -2\mathrm{Im}\ln\left[\frac{\sqrt{\lambda_3^* - \lambda_1^*} - \sqrt{\lambda_3^* - \lambda_1}}{\sqrt{\lambda_3^* - \lambda_1^*} + \sqrt{\lambda_3^* - \lambda_1}}\right],\\
&\xi = -2\mathrm{Re}\sqrt{(\lambda_3^* - \lambda_1)(\lambda_3^* - \lambda_1^*)},
\end{aligned} \tag{10}$$

with the assumption that $\mathrm{Re}\lambda_1 = -\mathrm{Re}\lambda_3 \to 0$ and $\mathrm{Im}\lambda_1 > \mathrm{Im}\lambda_3$. The selection of eigenvalues by using the rules in Eqs. (10) ensures that each λ_i belongs to the main spectrum. Now we can

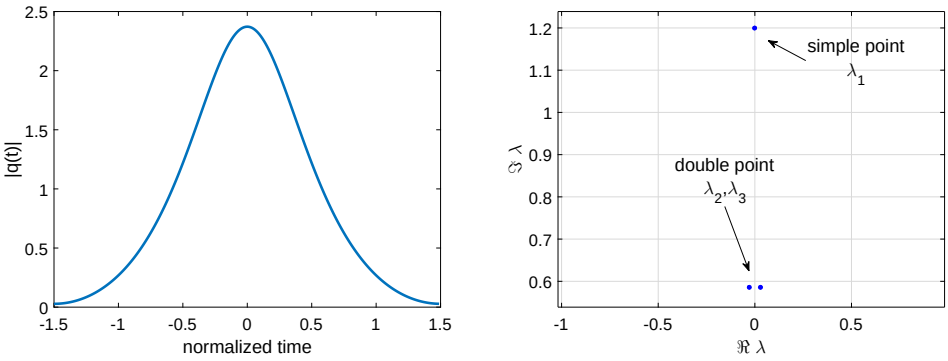

Fig. 2. The two-phase signal in Eq. (9) with $\lambda_1 = 1.2\,i$ (see the explanations in the text) and the time period $T_0 = 3$ defining the remaining values $\lambda_{2,3}$ (left). The corresponding main spectrum is shown in the right panel.

construct the signal by using Eq. (9) at $z = 0$ for different values of λ_1, and use the invariant value of λ_1 to encode and transmit our data. The value of λ_3 (and λ_2) is selected with respect to the chosen period of the signal T_0 by means of the relation: $\mathrm{Im}\lambda_3^2 = \mathrm{Im}\lambda_1^2 - \pi^2/{T_0}^2$, such that the resulting signals have the same period. Hence, the only data carrier parameter is the imaginary part of λ_1 which is drawn from a one dimensional constellation (like the one in Fig. 8 in Section 4 below). Fig. 2 depicts an example of such a signal and the corresponding main spectrum.

Since the two-phase signal of Eq. (9) is periodic, it can be recast as a Fourier series representation. The leading term of this series is by far larger than the succeeding one; the latter, in addition, can be made even smaller by decreasing the imaginary part of the eigenvalue. In this case, the bandwidth of different signals related to various values of eigenvalue remains almost constant. Thus, the important advantage of the periodic signals based on Eq. (9) is that it can be used to generate a set of encoded signals with similar characteristics, i.e. the similar bandwidth and time domain occupation (period).

In the case of the two-phase signal of Eq. (9) with two eigenvalues (located in the complex half-plane corresponding to positive imaginary parts, $\mathbb{C}^+$) since we intend to use only one of the points in the main spectrum, the area in which we can settle that point is limited by the positions of remaining points. So, the location of eigenvalues is confined, and hence, the power of different signals from the generated set varies insignificantly. For the example used in this work, the signal power varies between -1 dBm and 0 dBm for the smallest and largest eigenvalue respectively, set for signals with time duration of 0.42 ns giving the data rate 2.4 GSym/s. For the first time this signal was used in a PNFT-based communication in [22]. Now we have an alternative for the inverse transformation which provides us with adjustable period and one free point in the main spectrum, but the choices of power are limited and the main spectrum is restricted to a part of the imaginary axis. Because of the latter fact we can deal with the one dimensional constellations only. Note that the solution in Eq. (9) can also be obtained by means of a one-step Bäcklund transformation [23].

3.2. Perturbed plane wave

In the previous case, the main spectrum was confined to a part of the imaginary axis and we could use only one-dimensional constellations. To proceed one step forward for having two-dimensional constellations without calculating algebraic-geometric loop integrals [18, 19], one can use the analytical formulas given in [10, 19] derived for a special spectrum corresponding to a perturbed plane wave. As opposed to the two-phase signal of Eq. (9), the separation between

points in these pairs could be controlled, and this provides us with more degrees of freedom to design data-carrying eigenvalues forming our constellation.

A finite-gap periodic solution of NLSE can be constructed by carrying out the steps explained in Part I, subsection 4.2. For doing that one needs to find the Riemann spectrum, and this procedure is generally rather challenging. However, for the special cases of a perturbed plane wave the situation is much simpler [10]. The main spectrum of a plane wave $q(t) = A = \text{const.}$ in a time window T_0 (i.e. the PNFT period is T_0) consists of a simple (nondegenerate) point, $\lambda = A\,i$, and some double (degenerate) points on the real and imaginary axes, with their location given by:

$$\lambda_n' = \sqrt{\left(\frac{\pi n}{T_0}\right)^2 - A^2}, \qquad n < \frac{AT_0}{\pi}, \qquad n = 1, 2, \ldots . \tag{11}$$

Then, by adding a weak perturbation in the form of cosine waves to the initial constant waveform we can split up the degenerate points into the pairs of simple points (see Fig. 3). The main spectrum of the new waveform is characterized by the parameters: i) $\lambda = A\,i$, ii) the vector of g degenerate points of the plane wave $\boldsymbol{\lambda}'$ in Eq. (11), and iii) $\boldsymbol{\varepsilon}$, the vector with g elements determining the separation of the split points. For this main spectrum we can calculate the Riemann spectrum using the following formulas [10, 19] (see subsection 4.2. of Part I for the definition of Riemann spectrum parameters):

$$\begin{aligned}
&\boldsymbol{k} \approx -2\sqrt{A^2 + \boldsymbol{\lambda}'}, \quad \boldsymbol{\omega} = -2\boldsymbol{\lambda}' \odot \boldsymbol{k}, \\
&\tau_{jj} = \frac{1}{2} + \frac{i}{\pi} \ln\left(\frac{k_j^2}{\varepsilon_j}\right), \quad \tau_{lj} = \frac{i}{2\pi} \ln\left(\frac{1 + \lambda_l'\lambda_j' + 0.25 k_l k_j}{1 + \lambda_l'\lambda_j' - 0.25 k_l k_j}\right), \\
&\boldsymbol{\delta}^{\pm} = \pi + i \ln\left[\boldsymbol{\sigma} \odot (\boldsymbol{\lambda}' \pm \frac{1}{2}\boldsymbol{k}) \odot (\boldsymbol{\lambda}' + \frac{1}{2}\mathbf{k})\right],
\end{aligned} \tag{12}$$

where the vector of Riemann sheet indices, $\boldsymbol{\sigma}$, consists of ± 1s and $\odot$ is the element-wise multiplication. In fact, for small modulation amplitudes $\boldsymbol{\varepsilon}$, in the first order in $|\varepsilon_j|$ we have

$$q(t,0) = A + 2\sum_{j=1}^{g} |\varepsilon_j| \cos(k_j t + a_j) + O(\varepsilon^2). \tag{13}$$

where a_j are some phases, k_j are the elements of $\boldsymbol{k}$ from Eqs. (12) independent of $\boldsymbol{\varepsilon}$. Hence, if in a communication system based on this kind of signals our data mapped on the values of $\boldsymbol{\varepsilon}$, in this approximation all transmitted signals share the same bandwidth. Fig. 4 shows an example of such a signal where a degenerate point is split into two nondegenerate ones; for this figure we used $\varepsilon = 0.045 + 0.045i$ and $T_0 = 3.55$.

For this type of signals one can encode the data on the main spectrum by picking the complex values of the separations, ε_j, between the simple split eigenvalues. Since the analytical formulas of Eqs. (12) are derived in the first order of approximation in ε_j, we can control the modulation of the main spectrum only in the areas close to initial degenerate points, where the contribution of terms $\sim |\varepsilon|^2$ to these expressions are small. By picking the set of separations ε_j as complex values taken from an arbitrary constellation, we get the main spectrums in the form depicted in the right panel of Fig. 3, where one of the nondegenerate points and its mirrored one (with respect to a degenerate point of the plane wave, a blue dot in the left panel of Fig. 3) form the main spectrum.

Due to the noise-induced corruptions along the transmission, the received main spectrum becomes smeared. Thus, in order to minimise level of errors, it is necessary to have a sufficiently large minimum distance between the constellation points. However increasing the values of separations $|\varepsilon_j|$ one simultaneously decreases the accuracy of Eqs. (12) as these ignore the corrections $\sim |\varepsilon|^2$.

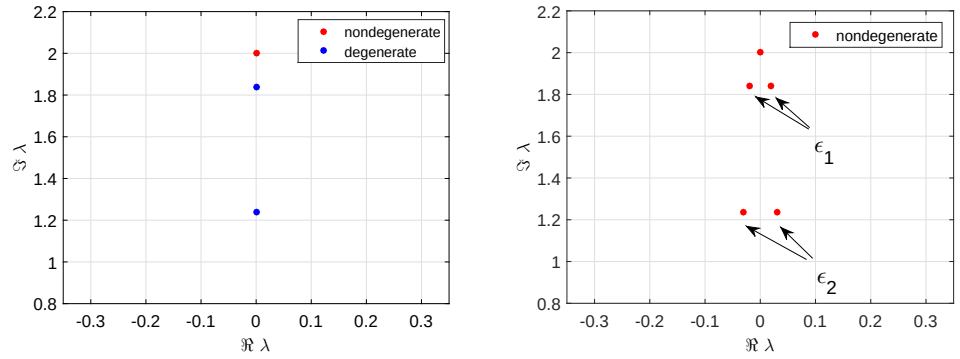

Fig. 3. Main spectrum of an unperturbed plane wave with $T_0 = 4$ and $A = 2$ (left), and a perturbed one with cosine waves with amplitudes ε_1 and ε_2.

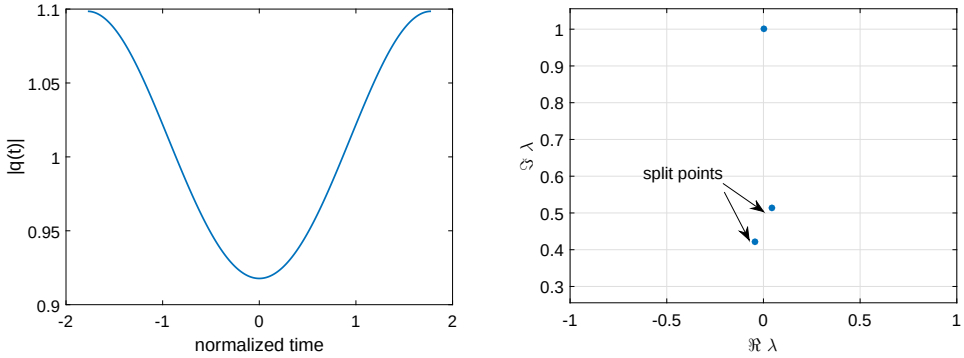

Fig. 4. Perturbed plane wave (subsection 3.2) with $\varepsilon = 0.045$ and period $T_0 = 3.55$ (left), and its main spectrum (right).

This is one of the current limitations of this approach in achieving high spectral efficiency communication system. Since the error in constructing the signal based on the chosen main spectrum of the form in Fig. 3 is deterministic, it is possible to equalize it at the receiver: as long as the deformation is not too large, one can replace the constellation points with the main spectrum of the initial signal. This new constellation will play the role of reference in the decision making stage of demodulation. Another solution to this problem is to use pilot symbols to equalize the received points at the receiver.

3.3. Modulated CW signal

One of the signals with known main spectrum is the plane wave $q(t) = Ae^{i\mu t}$ with period T_0, $\mu = k\pi/T_0$ with integer k. The main spectrum of this signal is a shifted version (for $-\mu/2$ along real axis) of the main spectrum of a plane wave with amplitude A and period T_0, i.e. of Eq. (11). Since μ and A determine the real and imaginary part of the points in the main spectrum respectively, one can make up a QAM constellation and map data on it to have a two dimensional constellation. Like the other above-mentioned signals, the requirement to have distinguishable points in the main spectrum entails the limited extent of variation for the imaginary part of points in main spectrum.

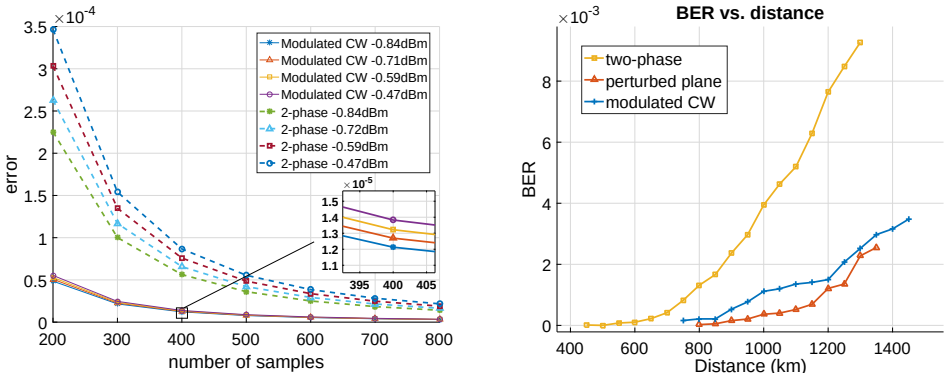

Fig. 5. Left: error vs. the number of samples in the B2B scenario for modulated CW and two-phase signals. Right: BER vs. distance in a single-symbol transmission with the constellation size $K = 64$ for modulated CW, two-phase and perturbed plane wave signals having -0.55 dBm power.

4. Simulation results

Now we assess the performance of eigenvalue communication system based on signal waveforms described in Section 3. Our criteria to quantify the performance of each system is the bit error rate (BER) value which is directly counted by the comparison of the transmitted and received bit sequences.

For the initial set of simulations we evaluate the accuracy of the whole procedure of mapping data on the NS and their retrieving via the direct PNFT in a back-to-back (B2B) scenario. The left panel of Fig. 5 shows the B2B error for a two-phase and a modulated CW signals for different powers. For these two signals the constellation is formed on an imaginary area between $1.2i$ and $1.5i$. These constraints are imposed to make the points of the main spectrum to be distinguishable from symbol to symbol: since the main spectrum for each symbol comprises more than one point (among which only one bears our data), so we have to be capable to distinguish between them. This figure shows the improvement in the B2B procedure performance with the increase in the number of samples and the decrease of power, both effects are basically due to the numerical AL PNFT routine functioning. The performance for the modulated CW is better signal than that for the two-phase one. Since for the perturbed plane wave we are going to equalize the received signal, i.e. to use the distorted main spectrum of the constructed signal at the transmitter as the reference constellation at the receiver, the B2B performance does not correctly characterize the error, and thus it is not depicted in our figure. From Fig. 5 (left), we see that setting the number of samples (per period) to be ≈ 500 should be sufficient for an accurate system functioning to avoid a noticeable contribution from the PNFT numerical error at the receiver.

In our fiber simulations in Eq. (1) we use the typical parameters $\beta_2 = -21.67\,\mathrm{ps}^2/\mathrm{km}$ and $\gamma = 1.27\,\mathrm{W}^{-1}\mathrm{km}^{-1}$. For each eigenvalue communication system we pick a point from the corresponding constellation, construct the signal having a desirable characteristics, and then launch it into the fiber. At the receiver, the main spectrum is calculated by performing the direct PNFT, the data is extracted and the resulting system BER is evaluated. To simulate the signal propagation down the fiber we use the split-step Fourier (SSF) routine setting a small enough step in z to ensure the adequate resolution. Since the SSF uses FFT to perform the linear filtering part of the evolution, the periodicity assumption is automatically fulfilled and, therefore, sending a single signal implies that we effectively have the exact periodicity of our pattern, or, in other words, we effectively have the infinite duration of our cyclic prefix (CP). Although a very large

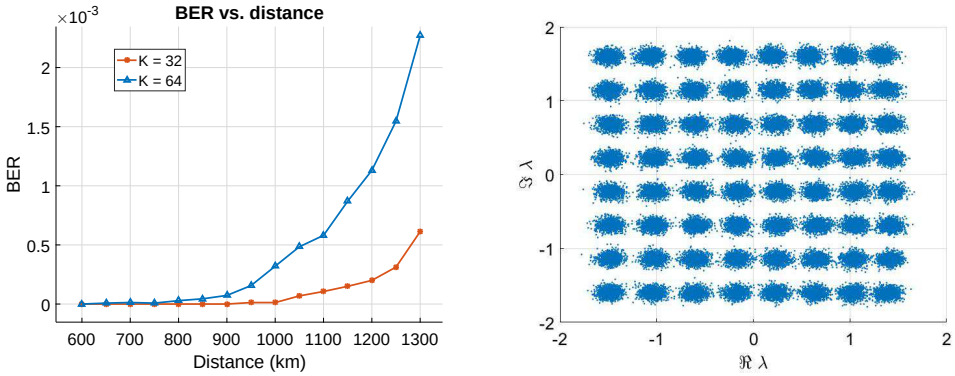

Fig. 6. BER vs. distance, for 32 and 64-QAM constellations made up by using the perturbed plane wave profile (Subsection 3.2), with -0.5 dBm power, CP$=$ 110% (left), and its received 64 QAM constellation at the propagation distance 1000 km (right).

CP values are not practical, reducing the spectral efficiency of the communication system, by studying this case one illustrates the singled out impact of the nonlinear beating between noise and signal's NS on the transmission. This means that by setting an effectively infinite CP we are actually finding an upper bound for the performance of a realistic system that would otherwise additionally suffer from the ISI. The right panel of Fig. 5 depicts the BER of three purely periodic signals vs. the propagation distance for the constellation size $K = 64$, signal power -0.55 dBm and symbol rate 2 GSym/s. For a perturbed plane wave (subsection 3.2) we picked the QAM constellation, from which the separation parameters ε_i were drawn. Such a low transmission rate is chosen to limit the ISI caused by signal broadening in the continuous transmission mode. As was expected, due to the larger minimum distance between points in the main spectrum provided by two-dimensional constellations, the perturbed plane wave and the modulated CW signal revealed a better performance as opposed to the two-phase signal with the shortest minimum distance, rendering the largest BER.

The results described above addressed the analysis of noise impacts on the PNFT-based communication system performance. Now, in the next set of simulations we send a continuous train of signals equipped with cyclic extensions (i.e. with the CP inserted in-between them). To analyze the joint action of the noise and ISI impact on the system, we consider a signal train consisting of 64 consecutive encoded signals. The value of the CP is opted for as to exceed the channel dispersion-induced memory up to 1000 km; this memory, in turn, depends on the bandwidth and varies for different signals [24]. The left panels of Figs. 6–8 present the BER vs the propagation distance for the perturbed plane wave signal (Subsection 3.2), modulated CW signal (Subsection 3.3) and two-phase signal in Eq. (9) respectively, for different sizes of constellation in a continuous transmission mode. As it can be seen from the figures, as far as the CP value is bigger than the dispersion-induced signal broadening, the functionality of the continuous mode is the same as we had in a single-symbol mode with infinite CP. To suppress the out of band noise we filter the signal in a bandwidth containing 99% of signal power which for the perturbed plane wave signal (Subsection 3.2) is 2 GHz (giving rise to the 110% CP), for modulated CW signal (Subsection 3.3) is roughly 4 GHz (giving rise to the 250% CP) and for the two-phase signal of Eq. (9) is 3 GHz (giving rise to the 200% CP). The optimum signal power of a conventional system in the same fiber is much higher than -0.55 dBm, which makes our system to perform in an essentially nonlinear regime [8].

In communication systems the noise influence on the performance is usually manageable by adjusting the signal power, thus changing the signal-to-noise ratio (SNR). When one have dis-

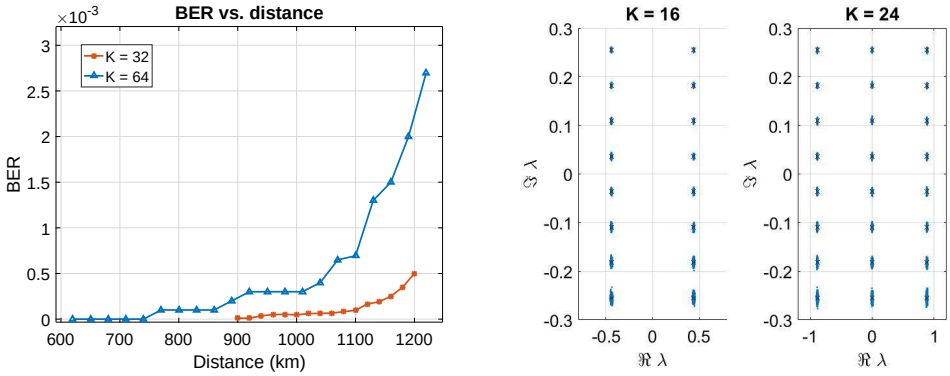

Fig. 7. BER vs. distance, for 32 and 64-QAM constellations made up by using the modulated CW wave (Subsection 3.3), with -0.5 dBm power, CP$=$ 250% (left). Right pane shows the example received constellation for $K = 16$, 24, at the propagation distance 1000 km.

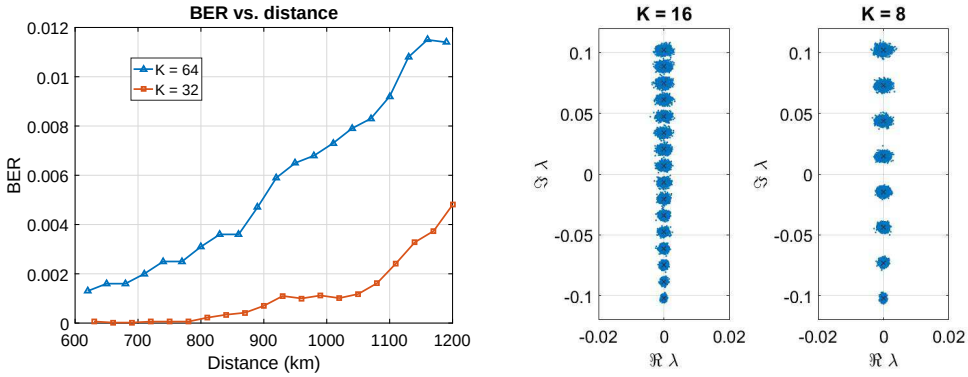

Fig. 8. BER vs. distance, for 32 and 64-QAM constellations made up by using the two-phase signal of Eq. (9), with -0.5 dBm power, CP$=$ 200% (left). Right pane shows the example received constellation for $K = 8$, 16, at the propagation distance 1000 km.

carded the auxiliary signal spectrum from the considerations, the signal power can be controlled by the imaginary part of the points that we pick in the main spectrum. Since the modulated CW and the two-phase signals used in our work are made up by using two sets of points in the main spectrum from which only one point carries our data, the fact that these two sets are separated only in the imaginary axis direction leaves a relatively small room for our altering the signal power. This means that the increase in the spectral efficiency can be rendered by increasing the constellation size only in the real axis direction. The latter is impossible for the two-phase signal. For the modulated CW signal it means that one has to deal with the signals having a considerable different group velocity. The strong variations in the signal velocities, in turn, means that we are effectively gaining more ISI action during our transmission, and that is exactly the reason why the larger CP extent was applied for our modulated CW signal. For the perturbed plane wave, the signal power is adjustable by manipulating the value of ε, but, as was explained earlier, the large values of separations ε_j bring about the deterministic error coming from the inverse transform stage; the same difficulty appears when one adds new points along the real dimension. This condition puts a cap on the ultimate throughput of the system, although one can potentially avoid this difficulty adopting a more involved signal synthesis procedure, i.e. by the numerical calculation of the loop integrals (to synthesize signal from a given NS, as it was briefly explained

in Part I).

5. Conclusion

In this work, following the Part I we propose several designs of communication systems based on the PNFT method. Generally, one has to perform the inverse PNFT to synthesize a desirable encoded signal in the time domain. The generated signal is sent to the fiber, and at the receiver the initially encoded data are retrieved by applying the direct PNFT. In the proposed approach we simplified the task and substituted the inverse transform part with three alternatives with simpler implementation, namely: using two-phase and modulated CW signals with the analytically known NS, and using available analytical expressions for the special case of a perturbed plane wave. We note that the use of these signal waveforms sets some limitation on the form of the main spectrum leading to the restriction on power variation and the minimum distance between the constellation points. By performing the numerical simulations with the account of noise (assuming the ideal distributed amplification) we compared the performance of these designs in a single-symbol scenario, where only the noise source of errors was accounted for. In this idealistic scenario the modulated CW signals demonstrated the best performance. Next, we simulated the transmission of a continuous stream of symbols with added CP and evaluated the performance of the resulting system by calculating the total BER vs. the transmission distance. As expected, when the dispersion induced memory was lower that the value of CP, the performance of the systems was identical to that in the single-symbol mode. However, when the dispersion-induced memory had overgrown the CP value we observed a rapid performance degradation. We would like to point out that though our simulations showed the potential of employing the PNFT-based system designs for efficacious transmission, it can be improved further by directly carrying out the inverse transform step (as described in Part I) rendering the opportunity to have arbitrary main spectrum with adjustable and controllable characteristics.

Funding

This work was supported by the UK EPSRC Programme Grant UNLOC EP/J017582/1.